

# Estimation of Pressure Gradient Images from Velocity Encoded MR Acquisitions

A Herment, G Besson, C Pellot-Barakat, F Frouin

Inserm, UMR-S 678, LIF & UPMC Univ Paris 06, F-75013, Paris, France

## Abstract

Magnetic resonance imaging (MRI) offers the potential to estimate blood pressure gradients, by solving the Navier-Stokes model relating the haemodynamic pressure to the acceleration and velocity. Here we compared results directly obtained using acceleration encoded MR sequences with those calculated from MR velocity acquisitions available on clinical systems. We found that using velocity encoded data instead of acceleration encoded data significantly degrade gradient pressure images. Two experimental phantoms were used to separately evaluate the inertial and convective components of the acceleration. To improve the quality of the pressure gradient estimation, the regularization of the acceleration field, calculated from velocity encoded acquisitions was investigated. We also suggest to increase the temporal resolution while lowering spatial resolution to lessen motion artifacts.

## 1. Introduction

Blood pressure gradients reflect the arterial wall compliance as well as the relaxation and contractility of the left ventricle. Magnetic resonance imaging (MRI) offers the potential to estimate blood pressure gradients non-invasively, as a safe alternative to catheter-based methods.

Local pressure gradients can be estimated by solving the model of Navier–Stokes (NS), from acceleration and velocity fields [1]. The NS equation links the pressure gradient  $\nabla p$  to the acceleration  $a$ , the viscous term  $\mu \nabla^2 v$ , where  $v$  is the velocity, and the body forces  $f$ :

$$\nabla p = -\rho a + \mu \nabla^2 v + f \quad (1)$$

Here  $\rho$  (kg m<sup>-3</sup>) and  $\mu$  (Pa s<sup>-1</sup>) are the blood density and dynamic viscosity respectively. For *in vivo* applications, the effect of the viscous term predominates in the close vicinity of the vessel wall at the blood–tissue interface and can thus be omitted in large vessels [2]. Since the patient lays down in the magnet, the body force term, which usually depends on the gravity, can also be neglected. Therefore

$$\nabla p = -\rho a. \quad (2)$$

Acceleration encoding is made possible by replacing the bipolar velocity-encoding gradient used in MR phase contrast imaging with a tripolar acceleration-encoding gradient. The feasibility of computing pressure variations from acceleration data has been validated in the aorta and cardiac chambers [3-5]. However most systems do not allow this acceleration encoding gradient. Due to the availability of velocity data acquisitions on clinical MR systems, velocity-encoded rather than acceleration-encoded acquisitions are generally used [6-10]. The acceleration field,  $\hat{a}$ , is then calculated from the velocity data  $v$  as follows:

$$\hat{a} = \frac{\partial v}{\partial t} + v \nabla \cdot v \quad (3)$$

where  $\frac{\partial v}{\partial t}$  represents the inertial acceleration term and  $v \nabla \cdot v$  the convective acceleration term.

Derivations with respect to time and space (Eq. 3) amplify noise in computed acceleration maps. Furthermore, motion of cardiovascular structures can also provide a biased estimation of  $\frac{\partial v}{\partial t}$ .

This paper describes a study of the degradation of acceleration images estimated from velocity data and provides an alternative to restore acceleration map quality.

## 2. Material

Two phantoms were built to study separately the inertial and the convective components of the acceleration when computing acceleration from velocity maps.

### *Inertial phantom*

The inertial term was studied with a pulsatile flow phantom [5] made of a long (2.4 m) flexible nylon tubing (inner diameter 3.2 cm, wall thickness 0.8 mm). The tube was filled with a water and glycerol mix to simulate the viscosity of blood. Pulsatile flow (98 bpm) was generated by using a calibrated motorized piston. The long entry

section of the tubing and the compliance of the tube (3 mm in diameter variation for a 70 mmHg pressure variation) provided a quasi-laminar flow. The inertial acceleration component in the  $z$  direction was then computed as:

$$\hat{a}_z = \frac{\partial v_z}{\partial t} + v_z \frac{\partial v_z}{\partial z} \quad (4)$$

A blunt flow profile was generated to study temporal derivation effects thus  $v_z \frac{\partial v_z}{\partial z} = 0$  and  $\hat{a}_z = \frac{\partial v_z}{\partial t}$ . A parabolic flow profile was also modelled from these data to estimate the bias generated by structure motion with time.

#### Convective phantom

The phantom used for this second study was a 20 mm thick and 270 mm diameter rotating cylinder, made of Altuglass and filled with agar gel [4]. One characteristic of this phantom is that the out-of-plane velocity  $v_z$  and acceleration  $a_z$  were zero. The angular velocity  $\omega$  was constant, so that the temporal derivative of the velocity was zero. The two in-plane convective components of the acceleration field were thus calculated as :

$$\begin{cases} \hat{a}_x = v_x \frac{\partial v_x}{\partial x} + v_y \frac{\partial v_x}{\partial y} \\ \hat{a}_y = v_x \frac{\partial v_y}{\partial x} + v_y \frac{\partial v_y}{\partial y} \end{cases} \quad (5)$$

#### Acquisitions

All images were acquired on a 1.5 T Signa magnetic resonance (MR) imager (GE Healthcare, Milwaukee, WI) with standard body and gradient coils. A gradient echo sequence was used in which a bipolar velocity-encoding gradient or a tripolar acceleration-encoding gradient was inserted between the rf pulse and the space-encoding phase and frequency gradients [1].

MR imaging was performed at a gradient strength of 10 mT m<sup>-1</sup> and a slew rate of 17 mT m<sup>-1</sup> s<sup>-1</sup>. Images were acquired with the following parameters: 256.128 spatial matrix and NEX = 1. The maximal velocity and acceleration-encoding values were, respectively,  $V_{enc} = \pm 360$  cm s<sup>-1</sup> and  $A_{enc} = \pm 4000$  cm s<sup>-2</sup>. These parameters yielded TR = 15 ms and TE = 7.5 ms for velocity encoding and TR = 24 ms and TE = 15.6 ms for acceleration encoding. The fields of view and flip angles were (14 cm, 30°) and (40 cm, 60°) for the flow phantom and the rotating phantom respectively. This allowed us to optimize image resolution and to compensate for the lower signal in agar gel compared to that in the water-glycerol mix.

The axes of the phantoms were aligned with the direction of the principal magnetic field. The slice thickness was 5 mm to obtain a precise spatial location while complying with *in vivo* applications. The acquisitions were synchronized on the signals delivered by the pumping and rotating motors. For in-vivo acquisitions, double oblique acquisitions were centered in a section including : the left atrium, the left ventricle and the primitive aorta. The same settings of the sequence were used except for  $V_{enc}$  and  $A_{enc}$  that were changed to  $\pm 180$  cm s<sup>-1</sup> and  $\pm 5000$  cm s<sup>-2</sup>

### 3. Methods

Derivatives in Eqs. (3-5) amplify strongly the acquisition noise. As usual for discrete time and space data, the derivatives were calculated by using a central difference approximation [6-10]. Furthermore the term  $v_x \frac{\partial v_x}{\partial x}$  as in Eq. (4) shows an amplification of noise with the value of the velocity itself. In order to improve the SNR, we implemented a regularization of the estimated acceleration. We used the classical approach of minimization of an energy function.

$$E_1 = \sum_{i,j,t} (\hat{\alpha}_{i,j,t} - \alpha_{i,j,t})^2 + \mu \sum_{i,j,t} [(\hat{\alpha}_{i,j,t+1} - \hat{\alpha}_{i,j,t})^2] \quad (6)$$

for the inertial components  $\alpha$  and

$$\begin{aligned} E_2 = \sum_{i,j,t} (\hat{\beta}_{i,j,t} - \beta_{i,j,t})^2 + \\ \mu \sum_{i,j,t} [v_{i,j,t} |((\hat{\beta}_{i+1,j,t} - \hat{\beta}_{i,j,t})^2 + (\hat{\beta}_{i,j,t+1} - \hat{\beta}_{i,j,t})^2)] \end{aligned} \quad (7)$$

for the convective terms  $\beta$ .

A conjugate gradient descent algorithm was used to minimize these energy functions.

### 4. Results

#### Inertial Phantom

Figure (1) shows a comparison between acceleration encoded acquisition and acceleration estimated from velocity encoded acquisitions. The degradation of inertial acceleration is visible and its improvement using regularization can be seen as well.

Figure (2) presents accelerations estimated between the phases 4 and 5 of the flow cycle for a parabolic flow profile with and without motion. The bias due to the motion can be seen on the estimated acceleration profiles, mainly on the borders.

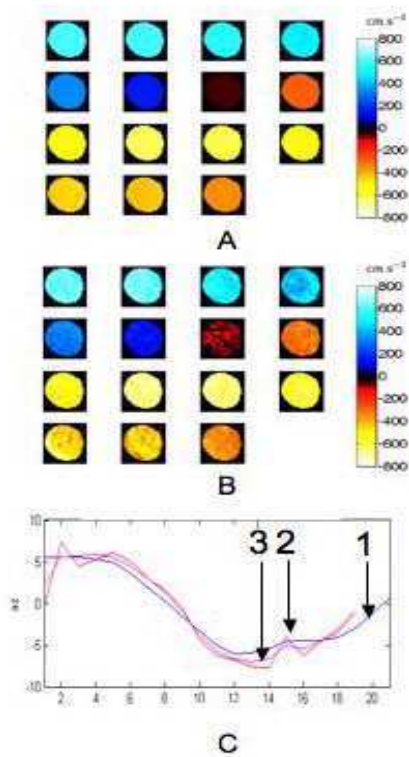


Fig.1 A) acceleration encoded acquisitions, B) acceleration calculated from velocity acquisitions. C) acceleration of the tube central axis versus time : 1) measured, 2) calculated, 3) calculated and regularized.

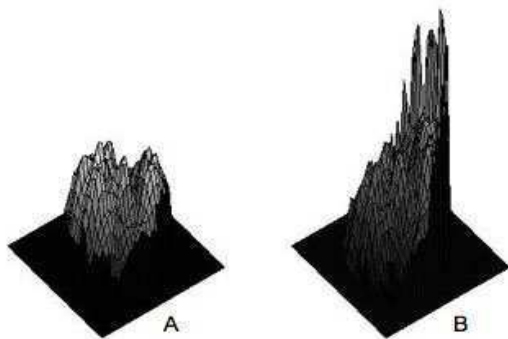


Fig.2 Acceleration calculated from velocity encoded acquisitions : parabolic flow profile. A) no motion, B) shift of one voxel between velocity phases 4 and 5.

*Convective phantom*

Figure (3) compares measured accelerations with accelerations estimated from velocity data, without and with regularization. The noise amplification with the velocity value, predicted in Eq. (5) is clearly visible on the second row. The impact of the velocity dependent regularization is well demonstrated.

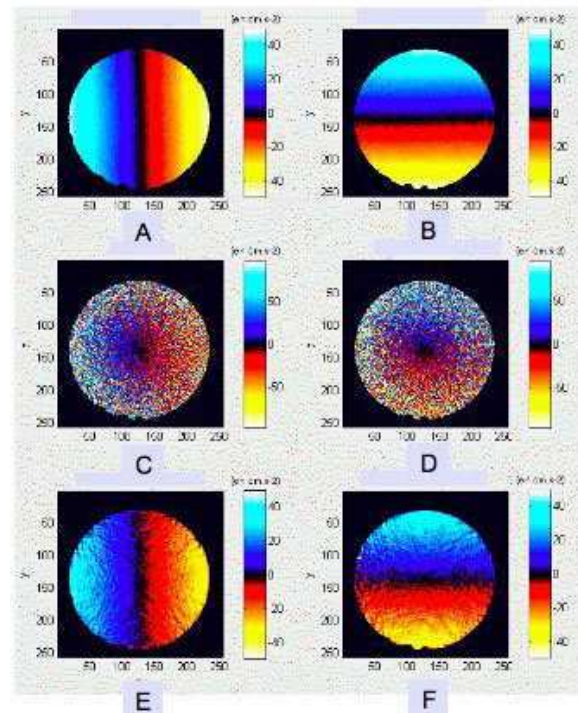


Fig.3 x and y components of the acceleration in the convective phantom. A), B) measured, C), D) calculated, E), F) calculated and regularized.

*Example of cardiac application*

Figure (4) compares telesystolic and telediastolic gradient pressure maps extracted from acceleration encoded acquisitions, velocity encoded acquisitions, without and with regularization.

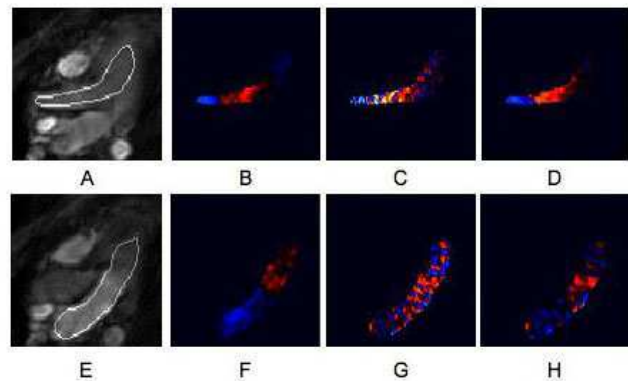


Fig.4 Cardiac example : telesystolic phase (top row), , telediastolic phase (bottom row). A) segmentation of the outflow track (left ventricle and aorta), E) segmentation of the filling path (left atrium and left ventricle). B), F) acceleration encoded acquisitions ; C), G) acceleration calculated from velocity encoded acquisitions ; D), H) velocity encoded acquisitions and regularization.

## 5. Discussion and conclusions

The use of direct MR measurements of the acceleration field for estimating pressure gradient maps was compared to that computed from MR velocity data.

### *Noise influence*

The results clearly show that, to obtain the particle acceleration in MRI, direct measurement of the acceleration field is preferable to calculation from velocity data, as the latter approach significantly degrades the signal-to-noise ratio.

When using acceleration or velocity encoding gradients, the noise variance of the information encoded in the MR signal phase is constant and depends only on the strength of the encoding gradient [11]. The results obtained by computing the convective acceleration from velocity data clearly indicate dependence on the noise variance of the acceleration with respect to the velocity of the moving element. An adapted regularization of the estimated acceleration data has shown to be quite efficient.

### *Flow regimen influence*

Flow characteristics also affect the SNR in the velocity and acceleration data. Any dispersion of particle velocities in a voxel (turbulent flows or rapid spatial variation of the flow profile) creates a phase shift of the encoded spins that degrades the SNR of the MR signal.

### *Motion influence*

Any motion of the heart or vessel between two successive phases of the cardiac cycle can result in a bias of the acceleration estimation because the time derivatives are no more calculated for the same position of the voxel. Modifying the MR acquisition sequence by increasing the temporal resolution and decreasing equally the spatial resolution can be used as an alternative. Shorter time gaps between images will reduce the motion of the flow voxel and a lower spatial resolution will provide « larger voxels » reducing the effect of motion as well. Finally increasing the voxel size improves the SNR of acquisitions which will in turn improve acceleration estimation.

## Acknowledgements

The authors are greatly thankful the U2R2M research centre for providing velocity and acceleration sequences and phantoms.

## References

- [1] Bittoun J, Jolivet O, Herment A, Itti E, Durand E, Mousseaux E and Tasu JP. Multidimensional MR mapping of multiple components of velocity and acceleration by Fourier phase encoding with a small number of encoding steps. *Magn Reson Med* 2000;44:723–30.
- [2] Wood NB. Aspects of fluid dynamics applied to the larger arteries. *J Theor Biol* 1999 ;137–61.
- [3] Buyens F, Jolivet O, De Cesare A, Bittoun J, Tasu JP, Herment A, Mousseaux E. Calculation of left ventricle relative pressure distribution in MRI using acceleration data. *Magn Reson Med* 2005;53:877–84.
- [4] Durand E, Jolivet O, Itty E, Tasu JP, Bittoun J. Precision of magnetic resonance velocity and acceleration measurements: theoretical issues and phantom experiments. *Magn Reson Imaging* 2001;13:445–51.
- [5] Tasu JP, Mousseaux E, Delouche A, Oddou C, Jolivet O, Bittoun J. Estimation of pressure gradients in pulsatile flow from magnetic resonance acceleration measurement. *Magn Reson Imaging* 2000;44:66–72.
- [6] Urchuk SN, Plewes DB. MR measurement of pulsatile pressure gradients. *Magn Reson Imaging* 1994;4:829–36.
- [7] Thompson R, McVeigh E. Fast measurement of intracardiac pressure differences with 2D breath-hold phase-contrast MRI. *Magn Reson Med* 2003;49:056–66.
- [8] Yang GZ, Kilner P, Woods N, Underwood R, Firmin D. Computation of flow pressure fields from magnetic resonance velocity mapping. *Magn Reson Med* 1996;36 : 520–6.
- [9] Tyszka J, Laidlaw D, Asa J, Silverman J. Three-dimensional, time-resolved (4D) relative pressure mapping using magnetic resonance imaging. *Magn Reson Imaging* 2002 ;12:321–29.
- [10] Ebbers T, Wigström L, Bolger AF, Engvall J, Karlsson K. Noninvasive measurement of time-varying three-dimensional relative pressure fields within the human heart. *J Biomech Eng* 2002;124:288–93.
- [11] Lamothe MJ, Rutt BK. Multistep phase difference phase contrast imaging. *Magn Reson Imaging* 1997;7:838–42.

Address for correspondence

Alain Herment

U678 Inserm, CHU Pitié, 91 Boulevard de l'Hôpital,

75013 Paris – France

herment@imed.jussieu.fr